ZANCO Journal of Pure and Applied Sciences

TYPE Original article
DOI http://dx.doi.org/10.21271/ZJPAS.38.3.12

OPEN ACCESS

*Corresponding author
Hemn Ameen Abduljabbar
hemnamin10@gmail.com

RECEIVED :14/09/2025
ACCEPTED :30/11/2025
PUBLISHED :30/06/ 2026

KEYWORDS:
Brain tumor, MRI, Segmentation, Adaptive clustering, Morphological refinement, FCM.

Unsupervised Brain Tumor Segmentation in MRI Using Adaptive Clustering and Morphological Refinement.

Hemn Ameen Abduljabbar* & Taban Fouad Majeed

Department of Computer Science and Information Technology, College of Science, Salahaddin University-Erbil, Erbil, Kurdistan Region, Iraq.

ABSTRACT

Segmentation and detection of brain tumors are some of the most difficult problems in medical imaging due to the complexity of brain tumor morphology and because they require manual annotation for segmentation. In this paper we have developed a new unsupervised clustering approach called Adaptive Clustering Morphological Refining (ACMR). ACMR uses a Fuzzy C-means (FCM)-based framework as well as an adaptive multi-clustering fusion approach. Our methodology includes anisotropic diffusion, novel FCM-Guided Contrast Limited Adaptive Histogram Equalization (CLAHE), entropy-based confidence map fusion as well as morphological refining for the proposed methodology. The proposed methodology was rigorously tested using 2D FLAIR slices from 2 benchmark datasets: BraTS-2017 (N = 210) and BraTS-2021 (N = 1251). ACMR achieved high average dice similarity scores of 81.02 % and 81.06 %, respectively, and a very low processing time of 0.20 s/slice. Statistical validation using the Wilcoxon Signed-Rank Test confirmed that both the FCM-guided CLAHE preprocessing as well as the adaptive multi-clustering fusion approach yielded statistically significant improvements ($p < 0.001$) over their respective baselines, establishing their essential contribution to accuracy. These results are competitive with, or superior to, recent synthesis-based unsupervised approaches (SynthTumour, 78.03% Dice). ACMR provides a robust, cost-efficient, and reproducible solution, successfully achieving a crucial trade-off between segmentation accuracy and speed for resource-constrained clinical environments.

1.Introduction

Early detection of brain tumors is important in reducing mortality and improving the quality of patient care for this type of cancer, which is a major type of tumor that requires the most sophisticated and technical medical evaluation to diagnose, treat, and manage (Nayla Faiq and Shahab Wahhab, 2025).

Automatic brain tumor segmentation is vital to provide precise information regarding the size and location of the tumor in order to facilitate rapid and accurate diagnoses, assist in developing personalized therapeutic plans, and monitor the effectiveness of ongoing treatments (Ullah et al., 2023). While manual delineation of tumors by an expert radiologist represents the gold standard in terms of accuracy, it is a very time-consuming and labor-intensive process that is subject to significant intra- and inter-rater variability and often leads to inconsistent results across different clinical sites (Ranjbarzadeh et al., 2021).

The growing interest in accurately and reliably quantifying tumors in clinical practices and trials led to the use of automatic segmentation methods to help automate the brain tumor segmentation process. As such, brain tumor segmentation has become a primary focus in the area of medical image analysis for nearly two decades (Abdulqadir Ismail, 2020). Unsupervised clustering techniques (K-means and Fuzzy C-Means (FCM)) have been particularly popular due to their ability to operate without the need for training data that has been manually labeled and are relatively fast and computationally inexpensive (Farnoosh and Noushkaran, 2022). The use of unsupervised clustering allows the pixels or voxels in the Magnetic Resonance Image (MRI) data to be rapidly grouped into clusters based upon their similarity, resulting in a fast and easily interpretable segmentation of the tumor. Unfortunately, these types of segmentation approaches are often inconclusive. K-means tend to produce poor edge quality and are unable to identify many subtle characteristics of the tumor, while FCM produces better edge quality, however, the algorithm is extremely sensitive to the presence of noise and intensity inhomogeneity in the MRI data (Farnoosh and Noushkaran, 2022).

Despite the limitations of unsupervised clustering, there is still much research being conducted that utilizes unsupervised clustering as a means of segmenting medical images. For example, Hersh Muhsin and Sardar Pirkhider (2022) were able to utilize K-means to perform the segmentation of leukemia cells. It was the inability to resolve the limitations of individual clustering methods, such as the poor edge quality produced by K-means or the extreme sensitivity to noise exhibited by FCM, that drove researchers to develop hybrid approaches to clustering. An example of a hybrid approach is found in the work of Nabeel and Sardar (2023), who used a combination of Fuzzy C-Means and K-Means to perform superior segmentation of thalassemia cells from images. These studies demonstrate the scientific necessity of combining simple clustering with sophisticated, multi-stage refinement techniques to produce a segmentation method that is clinically viable in terms of accuracy, thereby establishing a solid foundation for our proposed work.

In addition to the continued exploration of unsupervised clustering approaches, supervised deep learning approaches have dramatically changed the landscape of brain tumor segmentation. In particular, Convolutional Neural Networks (CNNs) have achieved state-of-the-art performance in benchmark communities, including the MICCAI BraTS Challenge (Baid et al., 2021). CNNs are capable of achieving high levels of segmentation accuracy by capturing multi-scale representations of feature sets within MRI images (typically achieving a Dice Similarity Coefficient (DSC) above 0.80) and are often comparable to, if not exceeding, human annotated data (Cardenas et al., 2017, Kaifi, 2024) However, CNN-based approaches have limitations. One limitation is the requirement of vast amounts of annotated training data that are both time consuming and expensive to collect (Baid et al., 2021, Bonato et al., 2025). A second limitation is the requirement of complex network architectures with millions of parameters that lead to extended training times, increased memory usage, and longer inference times (Ranjbarzadeh et al., 2021, Fawzi et al., 2021). These limitations hinder the deployment of CNN-based models in clinical environments where the available computing

resources are limited.

These findings illustrate a fundamental and persistent tradeoff in the field. Unsupervised clustering methods are generally faster and less expensive to train and test, and do not require large annotated datasets to function (Xu et al., 2019). However, these methods often lack the level of precision required in clinical applications. Conversely, deep-learning based methods, when trained with sufficient quantities of data, are able to achieve high levels of precision in segmenting tumors, but these methods are often slow to train, require large amounts of memory, and may not be suitable for large-scale clinical deployment or real-time segmentation tasks (Gupta and Mishra, 2024). This tradeoff highlights the urgent need for methods that balance the segmentation accuracy and speed of execution.

To fill the void left by current segmentation methods, we propose the Adaptive Clustering with Morphological Refinement (ACMR) framework. The ACMR framework employs three novel design components: (i) a cluster-guided preprocessing component that uses the fuzzy cluster data to refine the region of interest related to the tumor; (ii) an adaptive multi-clustering module that produces multiple candidate clustering and selects the best candidates via an entropy-weighted confidence map; and (iii) a morphological refinement component that refines the output from the fusion of the multiple candidate clustering into anatomically-consistent tumor masks. The ACMR framework seeks to improve the segmentation accuracy associated with unsupervised methods while retaining the scalability and low computational costs of those methods.

This study's ultimate objective is to develop and validate the ACMR framework as a highly effective, fully-unsupervised brain tumor segmentation framework for MRI images. We will also compare the performance of the ACMR framework against established segmentation frameworks on standard benchmark datasets BraTS-2017 and BraTS-2021 to assess its relative performance against traditional unsupervised clustering baseline methods and recently developed state-of-the-art unsupervised segmentation frameworks. The contributions of this study are two-fold: (i) Demonstrating ACMR produces higher Dice scores than other unsupervised segmentation methods; and (ii) Proving ACMR requires significantly fewer computations than supervised deep-learning-based segmentation methods and therefore increases the feasibility of automated segmentation in clinical workflows.

2. Materials and Methods

Our proposed ACMR segmentation framework consists of sequential self-contained stages, designed to improve unsupervised segmentation accuracy while maintaining computational efficiency. The overall process is illustrated in Figure 1.

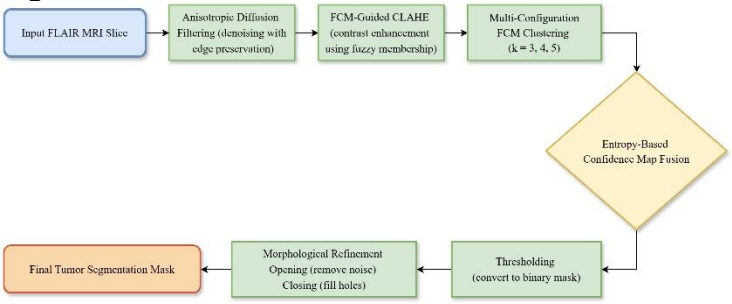

Figure 1. Overview of the ACMR Pre-processing and Segmentation Method

2.1 Dataset Description and Preparation

2.1.1 Dataset Used

Two publicly available, multi-institutional brain MRI datasets were utilized for model development and rigorous evaluation: the BraTS 2017 and BraTS 2021 training sets. From the original BraTS 2017 cohort (285 patients), we retained 210 High-Grade Glioma (HGG) cases for focused analysis (Alqazzaz et al., 2022). The full BraTS 2021 training set, consisting of 1,251 preoperative glioma cases, was used for primary benchmarking (Baid et al., 2021). The characteristics of BraTS 2017 and BraTS 2021 datasets are detailed in Table 1.

All data contained four co-registered 3D sequences; however, our study exclusively utilized the T2 Fluid Attenuated Inversion Recovery (FLAIR) volumes for each patient, as this modality offers optimal hyperintensity contrast for the entire tumor and surrounding peritumoral edema (Baid et al., 2021).

Table 1. Summary of datasets used in this study BraTS 2017 and BraTS 2021.

Dataset	Total Patients -Training Set	Used Patients	Modalities
BraTS 2017	285	210 HGG	T1, T1CE, T2, FLAIR
BraTS 2021	1251	1251	T1, T1CE, T2, FLAIR

2.1.2 Slice Selection

For each patient, a single representative 2D axial slice was extracted from the 3D FLAIR volume. This slice was identified using the ground-truth annotations as the one containing the largest tumor cross-sectional area. This process ensured that the evaluation was consistently performed on the most diagnostically relevant plane. The ground truth was used solely for this selection process and was not involved in the unsupervised segmentation methodology itself.

2.2 Pre-processing for Image Standardization

The ACMR pre-processing method enhances image quality by addressing noise and intensity inhomogeneities in a targeted manner.

2.2.1 FCM-Guided CLAHE

The most commonly used medical imaging technique for improving the local contrast of images is CLAHE (Stimper et al., 2019). in order to remove the localized effects of intensity variations, we developed an FCM-guided CLAHE, which limits the contrast enhancement to the hyper-intense tumor areas and prevents excessive enhancement of the homogenous surrounding tissues.

Initial FCM: FCM was first applied to the raw FLAIR image slice to cluster the image into a few clusters (k = 2) as fast as possible.

Target mask generation: the cluster with the highest intensity centroid, which consistently corresponds to the tumor and edema on FLAIR, was selected to create a target mask.

Targeted CLAHE: standard CLAHE (clip limit of .03 and 3x3 tile size) was applied only inside the previously created target mask area; therefore, the background pixels remained at their original intensity distributions. This method has been able to generate a tumor centric image with significantly enhanced borders to allow for additional clustering after this step.

2.2.2 Anisotropic Diffusion Denoising

Following this contrast adjustment, a Perona Malak Anisotropic Diffusion filter has been used to suppress image noise whilst preserve anatomical edge structure in the input images (Khmag, 2023) after the use of the FCM Guided CLAHE algorithm on the images. The filter was run for 3 iterations with both the conductivity parameter (k = 15), and time-step (λ = 0.17) being analytically determined to produce effective trade-offs between noise removal and preservation of anatomical detail.

2.3 Adaptive Multi-Clustering and Fusion

2.3.1 Multi-Configuration Clustering Strategy

This method was developed by an Adaptive Multi-Clustering (AMC), which overcame the major drawbacks of single-configuration FCM model. AMC utilizes heterogeneity in the size, location and intensity characteristics of the brain tumors as seen in different imaging environments (Bhimavarapu et al., 2024). Multiple FCM configurations are run in parallel within the AMC technique to capture many levels of tissue heterogeneity and tumor characteristics; therefore, eliminating the necessity of selecting the appropriate number of clusters a priori for the tissue.

This multi-configuration method is intended to provide a stable tumor margin identification capability against the large variability in both intensity and image quality found in the BraTS dataset from a variety of institutions. Utilization of ensemble clustering methods to improve discrimination capabilities in medical images is consistent with this strategy (Cetin-Kaya and Kaya, 2024).

FCM was run on the pre-processed image three

times with the use of cluster counts of k = 3, 4, and 5.

Reasons for choice of k values: The specific k value chosen (k = 3, 4, and 5) ensures that no matter what quality or level of noise is present in the slice, there is at least one configuration that can produce an effective representation of the whole tumor margin. The lowest k (k = 3) produces a more general and stable clustering of pixels into Background, Healthy Tissue, and Tumor. This type of clustering is best suited to slices with a high degree of noise or low contrast (Wen-qua, 2014). For example, the use of k = 3 instead of a larger k would prevent fragmentation when attempting to perform a more complex clustering of the tumor due to high noise or low contrast. On the other hand, the larger k values (k = 4 and k = 5) produce a finer discrimination between the tumor and the surrounding parenchyma, which is needed for high quality slices with high contrast. The tumor boundary in these types of slices is very subtle and requires a more sensitive separation than can be produced with a k = 3. A confidence map $C_i(x,y)$ is produced for each configuration which represents the membership value of pixel (x,y) to the identified whole tumor cluster (the cluster with the highest centroid intensity).

2.3.2 Entropy-Based Confidence Map Fusion

The individual confidence maps are integrated into a single, unified map using an adaptive weighting scheme. First Entropy Calculation ($\boldsymbol{H_i}$) is performed on the binary result of each configuration to quantify its uncertainty. Second, Adaptive Weighting ($\boldsymbol{w_i}$) is calculated as the inverse of entropy, such that configurations with lower uncertainty contribute a greater influence to the final fused map (Lu et al., 2019). The weighting is calculated as:

$$\boldsymbol{w_i} = \frac{(\boldsymbol{H_i} + \boldsymbol{\epsilon})^{-1}}{\sum_{j=1}^{m}(\boldsymbol{H_j} + \boldsymbol{\epsilon})^{-1}} \qquad (1)$$

Finally, Weighted Fusion is applied: the final fused confidence map (C_{fused}) is generated by a pixel-wise combination of the weighted maps:

$$\boldsymbol{C_{fused}(x,y)} = \sum_{i=1}^{3} \boldsymbol{w_i} \,.\, \boldsymbol{C_i}\,(\boldsymbol{x},\boldsymbol{y}) \qquad (2)$$

2.3.3 Thresholding

The fused confidence map is binarized using a fixed, empirically derived threshold of $\tau = 0.47$ to generate the final segmentation mask $M_{binary}\,(x,y)$ (Kanmani and Marikkannu, 2018).

2.4 Morphological Refinement

In order to generate an anatomically correct mask, many morphologic operations can be used. The first step is to apply a Morphological Opening operation on a 5-voxel diameter disk-shaped structural element to eliminate smaller noise and false positive detection (Aleid et al., 2023). Next, a Morphological Closing operation is applied by a 3-voxel diameter disk-shaped structural element to close small holes that exist internally in the tumor (Fawzi et al., 2021). At this point, a Connected Component Analysis is done to ensure that there is a spatial relationship between all elements of the tumor. There should only be two large connected components remaining after analysis because most tumors clinically are either single or formed from one or two dominant fragments (Sauwen et al., 2017).

We did not apply any further smoothing or optimization at this point. For instance, no Gaussian smoothing nor any filter based on intensities were used because the goal was to maintain the sharp binary segmentation mask that resulted from the morphological and connectivity processing. A representation of how the ACMR segmentation technique was applied to an example BraTS-2021 case is illustrated in Figure 2; it demonstrates the entire process starting with preprocessing and the CLAHE intensity enhancements using FCM as a guide through to multi-configurations for clustering and fusion weighted by entropy to the final segmented result when compared with the reference.

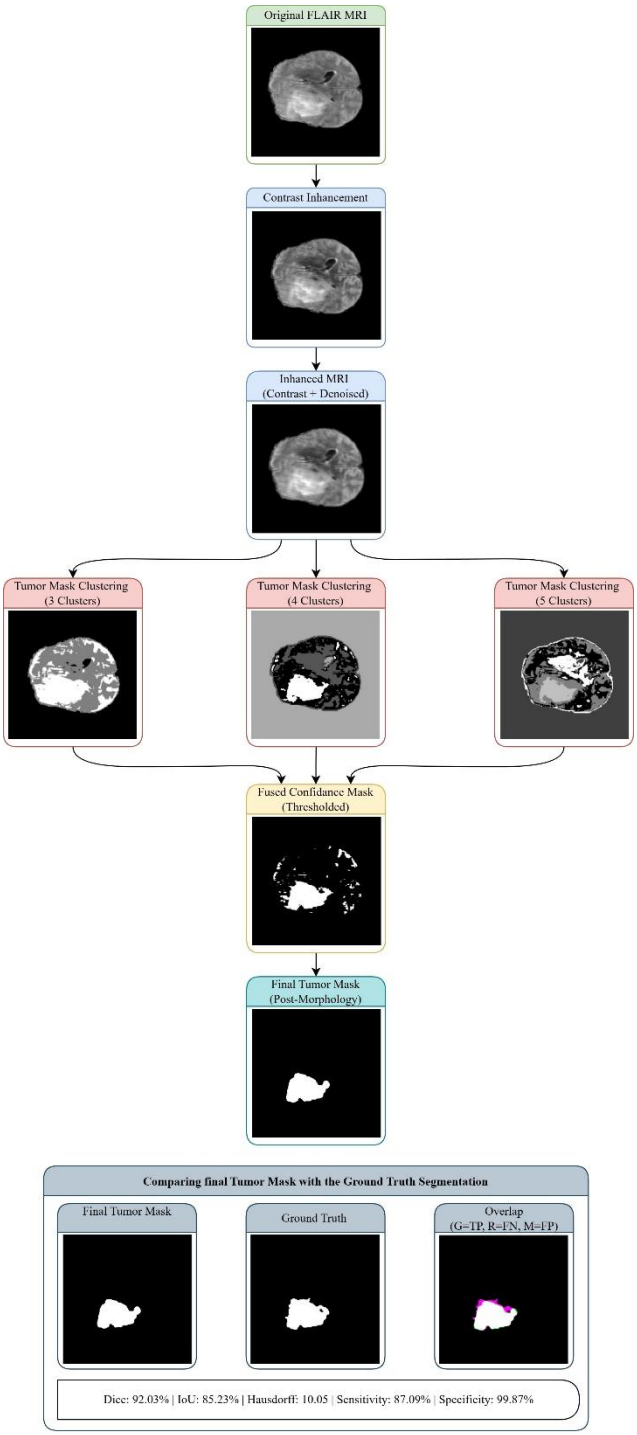

Figure 2. Visualization of the ACMR Segmentation Method for a Representative Case from the BraTS 2021 Dataset. The panels display the evolution from the initial image to intermediate masks and the segmentation when compared to ground truth.

2.5 Implementation Details and Statistical Analysis

2.5.1 Implementation Environment

Our proposed method was implemented in the MATLAB R2023b using Image Processing Toolbox and Parallel Computing Toolbox. Important steps - anisotropic filtering, FCM clustering, morphological refinement was accelerated to the extent possible on the GPU. Experiments were performed on a system that contains AMD Ryzen 7 7435HS (3.10 GHz) CPU and NVIDIA RTX 4060 (8 GB) GPU. The applicability of MATLAB to medical image segmentation has been shown in previous papers. Similarly, lung segmentation was carried out with MATLAB (Hamad and Majeed, 2022) and we have selected this environment for performing an efficient and repeatable analysis.

2.5.2 Statistical Analysis

To provide evidence for the reliability and validity of the suggested ACMR methodology, an explicit statistical evaluation was performed comparing the per-slice Dice scores obtained with the Proposed ACMR to those obtained with the Anisotropic Diffusion Only baseline via the Wilcoxon Signed-Rank Test (nonparametric paired test).

Validation of Pre-processing Design (FCM-Guided CLAHE): In the First Evaluation, the comparison of distributions of per-slice Dice scores obtained by the proposed ACMR compared to the distribution of Dice scores obtained by the Anisotropic Diffusion Only baseline on the BraTS 2017 dataset (N=210), was evaluated to show that the sequence of operations FCM-Guided CLAHE and adaptive multi-cluster processing significantly improved results over noise reduction alone, thus validating the pre-processing design.

Validation of Adaptive Multi-Clustering Strategy: In the Second Evaluation, the comparison of distributions of per-slice Dice scores obtained by the Proposed ACMR (Dice ~ 0.8106) versus the best performing individual configuration, Single FCM (k=3) (Dice ~ 0.7941), on the larger BraTS 2021 dataset (N=1,251), was analyzed to validate the statistically significant benefits of the Entropy-Based Confidence Map Fusion strategy as compared to any single clustering operation, thereby validating the adaptive nature of the multi-clustering approach.

2.6 Evaluation Metrics

All the segmentation evaluations were made at

the 2D slice level comparing each predicted tumor mask with its corresponding manually annotated ground truth mask from the BraTS 2017 and BraTS 2021 datasets. Baid et al. (2021) identified each ground truth slice was annotated by expert radiologists and metrics were computed per slice and not volumetrically. The following standard measures were used to numerically quantify segmentation performance:

2.6.1 Dice Similarity Coefficient (DSC)

The DSC was used to measure the overlap between the predicted segmentation mask *P* and the ground truth mask *G*. It is defined as:

$$\boldsymbol{Dice(P,G) = \frac{2|P \cap G|}{|P| + |G|}} \qquad (3)$$

where |*P*| and |G| represent the number of pixels in the predicted and ground truth masks, respectively, and |*P*∩*G*| is the number of overlapping pixels. A Dice value of 1 indicates perfect agreement, while 0 indicates no overlap (Taha and Hanbury, 2015, Ma et al., 2024)

2.6.2 Intersection-over-Union (IoU)

The IoU, also known as the Jaccard index, evaluates segmentation accuracy by measuring the ratio of overlap to the union between the predicted and ground truth masks:

$$\boldsymbol{IoU = \frac{|S_{pred} \cap S_{gt}|}{|S_{pred} \cup S_{gt}|} = \frac{TP}{TP + FP + FN}} \qquad (4)$$

This metric ranges from 0 to 1, where higher values indicate better segmentation overlap. IoU is stricter than Dice because it penalizes both false positives and false negatives more heavily (Rezatofighi et al., 2019).

2.6.3 Hausdorff Distance (HD)

HD quantifies the worst-case boundary error between the predicted mask *P* and ground truth *G*. For point sets *A*, *B* with distance *d*(·,·):

$$\boldsymbol{H(A,B) = \max\left(sup_{a \in A}\, inf_{b \in B}\, d(a,b), sup_{b \in B}\, inf_{a \in A}\, d(b,a)\right)} \qquad (5)$$

The inner *inf* finds the nearest boundary point; the outer *sup* selects the farthest mismatch. Smaller HD means better boundary alignment (Taha and Hanbury, 2015).

2.6.4 Sensitivity (Recall)

Sensitivity, also called recall or true positive rate, measures the proportion of actual tumor pixels correctly identified by the model. It is given by:

$$\boldsymbol{Sensitivity = \frac{TP}{TP + FN}} \qquad (6)$$

where TPTPTP is the number of true positives and FNFNFN is the number of false negatives. A higher sensitivity indicates better ability to detect tumor regions (Taha and Hanbury, 2015).

2.6.5 Specificity

Specificity, or true negative rate, quantifies the proportion of healthy (non-tumor) pixels correctly identified as negative. It is defined as:

$$\boldsymbol{Specificity = \frac{TN}{TN + FP}} \qquad (7)$$

where *TN* is the number of true negatives and *FP* is the number of false positives. High specificity ensures that non-tumor tissues are not falsely segmented as tumor regions (Muller et al., 2022).

3. Results

For the purpose of validating the accuracy and efficiency of the ACMR method, our proposed method was tested on both the BraTS-2017 and BraTS-2021 cohorts of brain tumors. To detail the primary quantitative outcomes of both validation cohorts, refer to the Table 2.

ACMR has been consistently successful in testing across multiple datasets, with an average Dice score of 81.02% BraTS 2017 and 81.06% BraTS 2021.

In order to formally determine the effectiveness of each of the novel components of this framework, a formal statistical evaluation was conducted. The preliminary comparative results of the ablation study, focusing on the BraTS-2017 dataset are contained within Table 3, while the results detailing the performance differences between single cluster and multi-cluster configurations can be seen in Figure 3.

A Wilcoxon Signed-Rank Test was used to formally evaluate the efficacy of both the preprocessing and clustering techniques by evaluating the Dice scores on a per-slice basis. The primary statistical results of these tests are contained in Table 4.

Evaluating the Effectiveness of FCM-Guided CLAHE: The entire ACMR method, including the FCM-Guided CLAHE preprocessing technique,

resulted in a statistically significant improvement in the Dice score when compared to the Anisotropic Diffusion Only baseline in the BraTS 2017 cohort ($p < 0.001$). Therefore, this study formally establishes that utilizing fuzzy clustering membership to enhance the tumor margin prior to segmentation is an effective and essential process.

Evaluating the Effectiveness of Adaptive Multi-Clustering: Utilizing the larger BraTS 2021 cohort, it was found that the Adaptive Multi-Clustering technique exhibited a statistically significant improvement in performance when compared to the best single configuration, Single FCM ($k = 3$) ($p < 0.001$). This further establishes the effectiveness of ensemble clustering for achieving robust segmentation and the ability of the ACMR algorithm to provide stable segmentation results in the presence of the inherent intensity variability present in MRI data.

Performance and efficiency contextualization illustrated in Table 5, the performance of ACMR was contextualized against the recent state-of-the-art unsupervised algorithms, demonstrating the competitive nature of both accuracy and processing time of ACMR. Specifically, on the large BraTS-2021 cohort (N = 1251) the ACMR algorithm demonstrated a very high Dice score of 81.06%, while demonstrating a competitive processing time of 0.20 seconds/slice. Therefore, due to the high accuracy and low processing requirements of ACMR, it presents a highly viable alternative for researchers and clinicians who do not have access to high-performance computing capabilities.

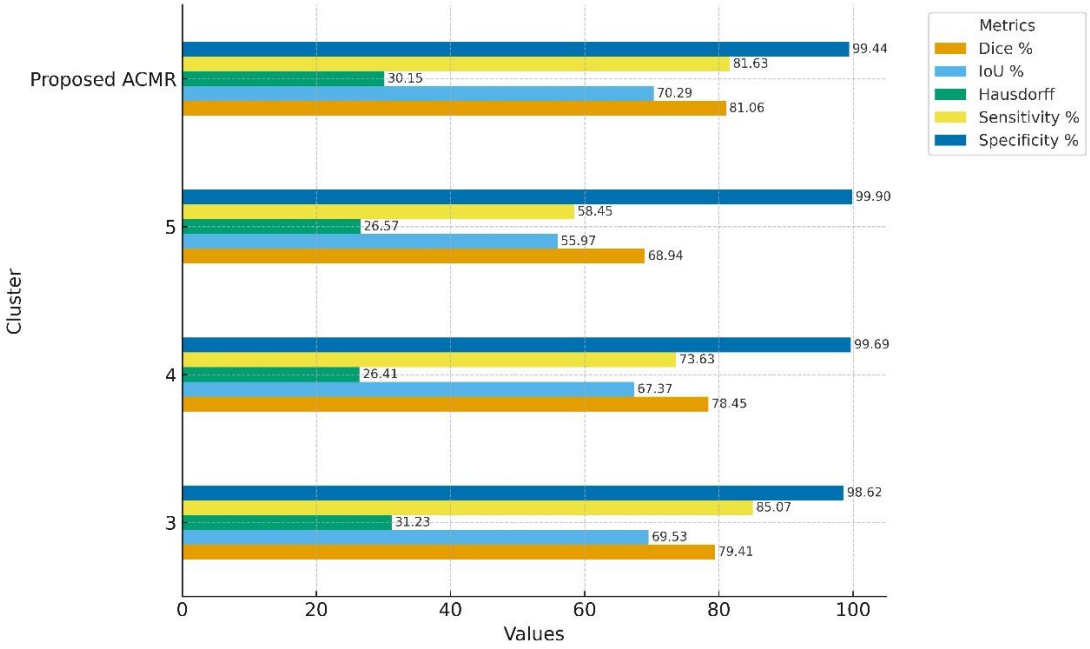

Figure 3. Performance metrics of single-clustering (k = 3, 4, 5) compared with the proposed ACMR method, showing ACMR achieves the highest Dice score (81.06%).

Table 2. Quantitative Performance of the ACMR Method on BraTS 2017 and BraTS 2021 Datasets.

Dataset	No. of Patients	Dice (%)	IoU (%)	Hausdorff Distance	Sensitivity (%)	Specificity (%)	Time Elapsed (s/slice)
BraTS 2021	1251	81.06	70.29	30.15	81.63	99.44	0.195
BraTS 2017	210	81.02	69.71	27.76	80.59	99.49	0.209

Table 3. Comparative analysis of pre-processing techniques on the BraTS 2017 Dataset.

Pre-processing Method	Dice (%)	IoU (%)	Hausdorff Distance	Sensitivity (%)	Specificity (%)
Anisotropic Diffusion Only	76.75	65.19	25.38	73.52	99.41
Original CLAHE + Anisotropic Diffusion	57.08	42.09	40.43	48.05	99.58
Proposed ACMR	81.02	69.71	27.76	80.59	99.49

Table 4. Statistical Validation of ACMR's Core Contributions

Comparison	**Dataset (N)**	**Mean Dice (ACMR)**	**Mean Dice (Baseline)**	**Dice Improvement (Δ)**	**SD (±)**	$p - value$	**Conclusion**
FCM-Guided CLAHE (vs. AD Only)	BraTS 2017 (210)	0.8102	0.7675	0.0427	0.052	p < 0.001	Significant Improvement
Adaptive Multi-Clustering (vs. Single FCM $k=3$)	BraTS 2021 (1,251)	0.8106	0.7941	0.0165	0.021	p < 0.001	Significant Improvement

Table 5. Comparison of ACMR with State-of-the-Art Unsupervised Segmentation Methods

Method	**Approach**	**Dataset (N)**	**Dice Score (%)**	**Runtime (s/slice)**
Hard and Soft Clustering (Bora and Mishra, 2025)	K-Mean (Hard Clustering)	BraTS 2020 (N/A)	43.0	0.30
	FC-mean (Soft Clustering)	BraTS 2020 (N/A)	67.0	1.30
SynthTumour (Zhang et al., 2025)	Two-Stage Image Synthesis (CNN-based)	BraTS 2021 (1,151)	78.03	Not Reported
ACMR (Proposed)	FCM, Multi-Clustering, Morphological Refinement	BraTS 2021 (1,251)	81.06	0.20

4. Discussion

ACMR's reliability and efficiency as an unsupervised solution for brain tumor segmentation was supported by the high Dice scores and short inference times as found in Section 3. ACMR's consistency in performance across both of the diverse sets of data BraTS-2017 and BraTS-2021 provides evidence that it can adequately handle many of the variabilities present in MRI studies (e.g., scanners and imaging parameters).

As indicated by the statistical results, the importance of the pre-processing stage is further emphasized by the comparison. As shown in Table 4, this analysis showed that the addition of the novel FCM-Guided CLAHE to the simple Anisotropic Diffusion-only baseline yielded a statistically significant improvement ($p < 0.001$). This validation of the central hypothesis of the study supports the idea that using fuzzy clustering membership to enhance contrast specifically related to tumors will be essential to achieving satisfactory unsupervised segmentation results. The results obtained from this study corroborate previous studies indicating limitations of global-based methods of contrast enhancement when applied to heterogenous medical images.

Also, the structural component of the Adaptive Multi-Clustering is statistically substantiated. In comparing ACMR to the single configuration that performed best (Single FCM, $k = 3$), the fused approach was determined to be statistically better than ($p < 0.001$) the single configuration. Although each individual cluster configuration may be

vulnerable to local noise or changes in intensity, the incorporation of entropy-weighted fusion into ACMR helps stabilize the convergence of boundaries to the tumors. Therefore, the ensemble strategy used in ACMR minimizes the potential for suboptimal segmentation decisions when dealing with variable glioma morphologies and thus, increases the overall reliability of the results. In comparing the performance of ACMR (Table 5) to SynthTumour (Zhang et al., 2025), another unsupervised method that uses complex image synthesis, ACMR achieved a much higher percentage of overlap accuracy (81.06%) than did SynthTumour (78.03%). Additionally, the performance of ACMR was far greater than that of simple clustering methods (Bora and Mishra, 2025Bora and Mishra, 2025), which were able to achieve a Dice score of only (67.0%) on the same cohort. Most importantly, ACMR has a significantly faster computational efficiency of 0.20 s/slice than did the other clustering methods (1.30 s/slice), which makes ACMR a viable alternative for clinical or research applications where there is limited access to powerful computing resources. Thus, ACMR, with its statistically validated higher percentage of overlap accuracy and its superior computational efficiency, represents a highly viable solution for clinical or research applications requiring unsupervised brain tumor segmentation, yet limited by available computing power. The combination of adaptive clustering, cluster-informed contrast enhancement, and morphological refinement has provided the optimal balance between accuracy and efficiency for unsupervised brain tumor segmentation.

5. Conclusion

This study demonstrates the success of developing and testing an ACMR method for automatically segmenting MRI brain tumors without supervision. It was found that ACMR presents a robust statistical and fast computational solution, as it reaches the required balance between segmentation performance and computing efficiency to be useful in the clinic.

The proposed solution (that combines the use of FCM for guiding CLAHE, multi-clustering fusion, and morphological refining) achieves a mean Dice Coefficient of 81.06% on the BraTs-2021 dataset. The results obtained by using ACMR are competitive to, or better than those reported by many other recent methods for unsupervised brain tumor segmentation. The average processing time of the proposed solution is under 0.20 seconds per slice.

Based on the findings from this study, ACMR is considered to be a very promising tool for both clinical applications and research settings where limited resources exist. Future studies will include the extension of ACMR to three-dimensional image segmentation and its integration with supervised machine learning algorithms to obtain higher discrimination levels between different types of tumor sub-regions.

Acknowledgment

The authors did not receive any external funding nor have additional acknowledgments.

Funding

This research received no specific grant from any funding agency in the public, commercial, or not-for-profit sectors.

Conflict of Interest

The authors report that they have no known competing financial interest or personal relationships that could have been perceived to influence the work reported in this paper.

References

Abdulqadir Ismail, A. 2020. Brain Cancer Medical Diagnostic System Using Grey Scale Features and Support Vector Machine. *Zanco Journal of Pure and Applied Sciences,* 32**,** 40-48.

Aleid, A., Alhussaini, K., Alanazi, R., Altwaimi, M., Altwijri, O. & Saad, A. S. 2023. Artificial Intelligence Approach for Early Detection of Brain Tumors Using MRI Images. *Applied Sciences,* 13.

Alqazzaz, S., Sun, X., Nokes, L. D., Yang, H., Yang, Y., Xu, R., Zhang, Y. & Yang, X. 2022. Combined Features in Region of Interest for Brain Tumor Segmentation. *J Digit Imaging,* 35**,** 938-946.

Baid, U., Ghodasara, S., Bilello, M., Mohan, S., Calabrese, E., Colak, E., Farahani, K., Kalpathy-Cramer, J., Kitamura, F., Pati, S., Prevedello, L., Rudie, J., Sako, C., Shinohara, R., Bergquist, T., Chai, R., Eddy, J., Elliott, J., Reade, W. & Bakas, S. 2021. *The RSNA-ASNR-MICCAI BraTS 2021 Benchmark on Brain Tumor Segmentation and Radiogenomic Classification*.

Bhimavarapu, U., Chintalapudi, N. & Battineni, G. 2024. Brain Tumor Detection and Categorization with Segmentation of Improved Unsupervised Clustering Approach and Machine Learning Classifier. *Bioengineering (Basel),* 11.

Bonato, B., Nanni, L. & Bertoldo, A. 2025. Advancing Precision: A Comprehensive Review of MRI

Segmentation Datasets from BraTS Challenges (2012-2025). *Sensors (Basel),* 25.

Bora, D. J. & Mishra, M. K. 2025. Comparative Evaluation of Hard and Soft Clustering for Precise Brain Tumor Segmentation in MR Imaging. *Journal of Advances in Mathematics and Computer Science,* 40**,** 127–141.

Cardenas, C. E., Mohamed, A. S. R., Tao, R., Wong, A. J. R., Awan, M. J., Kuruvila, S., Aristophanous, M., Gunn, G. B., Phan, J., Beadle, B. M., Frank, S. J., Garden, A. S., Morrison, W. H., Fuller, C. D. & Rosenthal, D. I. 2017. Prospective Qualitative and Quantitative Analysis of Real-Time Peer Review Quality Assurance Rounds Incorporating Direct Physical Examination for Head and Neck Cancer Radiation Therapy. *Int J Radiat Oncol Biol Phys,* 98**,** 532-540.

Cetin-Kaya, Y. & Kaya, M. 2024. A Novel Ensemble Framework for Multi-Classification of Brain Tumors Using Magnetic Resonance Imaging. *Diagnostics (Basel),* 14.

Farnoosh, R. & Noushkaran, H. 2022. Application of a Modified Combinational Approach to Brain Tumor Detection in MR Images. *J Digit Imaging,* 35**,** 1421-1432.

Fawzi, A., Achuthan, A. & Belaton, B. 2021. Brain Image Segmentation in Recent Years: A Narrative Review. *Brain Sci,* 11.

Gupta, M. & Mishra, A. 2024. A systematic review of deep learning based image segmentation to detect polyp. *Artificial Intelligence Review,* 57**,** 7.

Hamad, Z. H. & Majeed, T. F. 2022. Lung Region Segmentation Using Modified U-Net Architecture. *EURASIAN JOURNAL OF SCIENCE AND ENGINEERING,* 8**,** 25-38.

Hersh Muhsin, O. & Sardar Pirkhider, Y. 2022. Automated segmentation of Acute Lymphocytic Leukemia (ALL) subtypes by the combination of color space conversion and K-means cluster. *Zanco Journal of Pure and Applied Sciences,* 34**,** 11-20.

Kaifi, R. 2024. Enhancing brain tumor detection: a novel CNN approach with advanced activation functions for accurate medical imaging analysis. *Front Oncol,* 14**,** 1437185.

Kanmani, P. & Marikkannu, P. 2018. MRI Brain Images Classification: A Multi-Level Threshold Based Region Optimization Technique. *J Med Syst,* 42**,** 62.

Khmag, A. 2023. Natural digital image mixed noise removal using regularization Perona–Malik model and pulse coupled neural networks. *Soft Computing,* 27**,** 15523-15532.

Lu, S., Gao, F., Piao, C. & Ma, Y. Dynamic Weighted Cross Entropy for Semantic Segmentation with Extremely Imbalanced Data. 2019 2019. 230-233.

Ma, J., He, Y., Li, F., Han, L., You, C. & Wang, B. 2024. Segment anything in medical images. *Nat Commun,* 15**,** 654.

Muller, D., Soto-Rey, I. & Kramer, F. 2022. Towards a guideline for evaluation metrics in medical image segmentation. *BMC Res Notes,* 15**,** 210.

Nabeel, J. A. & Sardar, P. Y. 2023. Automated Thalassemia cell image segmentation using hybrid Fuzzy C-Means and K-Means. *Zanco Journal of Pure and Applied Sciences,* 35**,** 22-33.

Nayla Faiq, O. & Shahab Wahhab, K. 2025. Enhancing Brain Tumor Classification Accuracy Using Deep Learning with Real and Synthetic MRI Images. *Zanco Journal of Pure and Applied Sciences,* 37**,** 126-149.

Ranjbarzadeh, R., Bagherian Kasgari, A., Jafarzadeh Ghoushchi, S., Anari, S., Naseri, M. & Bendechache, M. 2021. Brain tumor segmentation based on deep learning and an attention mechanism using MRI multi-modalities brain images. *Sci Rep,* 11**,** 10930.

Rezatofighi, H., Tsoi, N., Gwak, J., Sadeghian, A., Reid, I. & Savarese, S. 2019. *Generalized Intersection Over Union: A Metric and a Loss for Bounding Box Regression*.

Sauwen, N., Acou, M., Sima, D. M., Veraart, J., Maes, F., Himmelreich, U., Achten, E. & Huffel, S. V. 2017. Semi-automated brain tumor segmentation on multi-parametric MRI using regularized non-negative matrix factorization. *BMC Med Imaging,* 17**,** 29.

Stimper, V., Bauer, S., Ernstorfer, R., Scholkopf, B. & Xian, R. P. 2019. Multidimensional Contrast Limited Adaptive Histogram Equalization. *IEEE Access,* 7**,** 165437-165447.

Taha, A. A. & Hanbury, A. 2015. Metrics for evaluating 3D medical image segmentation: analysis, selection, and tool. *BMC Med Imaging,* 15**,** 29.

Ullah, F., Nadeem, M., Abrar, M., Al-Razgan, M., Alfakih, T., Amin, F. & Salam, A. 2023. Brain Tumor Segmentation from MRI Images Using Handcrafted Convolutional Neural Network. *Diagnostics (Basel),* 13.

Wen-Qua, Z. 2014. MRI image segmentation method based on anisotropic diffusion and spatial FCM. *Application Research of Computers*.

Xu, X., Wei, Q., Li, H., Wang, Y., Chen, Y. & Jiang, Y. 2019. Recognition of polymer configurations by unsupervised learning. *Phys Rev E,* 99**,** 043307.

Zhang, X., Ou, N., Liu, C., Zhuo, Z., Matthews, P. M., Liu, Y., Ye, C. & Bai, W. 2025. Unsupervised brain MRI tumour segmentation via two-stage image synthesis. *Med Image Anal,* 102**,** 103568.